Theory of edge-state optical absorption in two-dimensional transition metal dichalcogenide flakes

Maxim Trushin
Department of Physics, University of Konstanz, D-78457 Konstanz, Germany

Edmund J. R. Kelleher
Department of Physics, Imperial College London, London, SW7 2AZ, UK

Tawfique Hasan
Cambridge Graphene Centre, University of Cambridge, 9 JJ Thomson Avenue, Cambridge, CB3 0FA, UK

(Dated: February 23, 2016)

We develop an analytical model to describe sub-bandgap optical absorption in two-dimensional semiconducting transition metal dichalcogenide (s-TMD) nanoflakes. The material system represents an array of few-layer molybdenum disulfide crystals, randomly orientated in a polymer matrix. We propose that optical absorption involves direct transitions between electronic edge-states and bulk-bands, depends strongly on the carrier population, and is saturable with sufficient fluence. For excitation energies above half the bandgap, the excess energy is absorbed by the edge-state electrons, elevating their effective temperature. Our analytical expressions for the linear and nonlinear absorption could prove useful tools in the design of practical photonic devices based on s-TMDs.

PACS numbers: 78.67.-n,78.67.Bf,78.66.Sq

I. INTRODUCTION

In the last decade, following the discovery of graphene,[1] research of two-dimensional (2d) materials has experienced explosive growth. A 2d material represents an atomically thin solid flake, with optical properties qualitatively different from its three-dimensional (3d) parent crystal.[2,3] One of the largest families of 2d materials is the transition metal dichalcogenides (TMDs) that contains over 40 different forms, either metallic or semiconducting.[2] TMDs have the general formula MX_2, where M represents a transition metal, (e.g. molybdenum or tungsten), and X represents a chalcogen (e.g. sulfur, selenium, tellurium).[2,3] Single-layer MX_2 crystals are quasi-2d structures, containing a plane of metal (M) atoms covalently bonded between two planes of chalcogen (X) atoms, see Fig. 1a. In contrast to bulk semiconducting TMD (s-TMD) crystals, their monolayers typically exhibit a direct bandgap at visible or near-infrared frequencies, making them a suitable material for a range of photonic and optoelectronic applications.[2,4–6] In a direct bandgap semiconductor, with a pristine lattice and of infinite extent, photons with energies lower than the bandgap cannot excite direct interband transitions; thus, single-photon absorption at these energies does not occur. Recent experiments by several research groups, however, have demonstrated both non-negligible linear absorption at sub-bandgap photon energies, as well as a finite nonlinear optical response in a variety of s-TMDs, including MoS_2[7,8], WS_2[9,10], $MoSe_2$.[11,12] Liquid phase exfoliated $MoSe_2$-polymer composites, for example, have been reported to exhibit >7% linear absorption in the 0.65–0.8 eV range,[11] in spite of $MoSe_2$ having a direct (in monolayer form) and indirect (bulk) bandgap of ∼1.5-1.58 eV and ∼1.1 eV, respectively.[3,13]

Several mechanisms have been proposed to explain this phenomenon. Supported by first principle calculations, Wang *et al.* suggested that a reduction in the MoS_2 bandgap could be achieved by introducing crystallographic defect states.[14] The authors also suggested that defects could activate the material as a broadband saturable absorber.[14] We recently proposed that edge-states contribute to sub-bandgap absorption in s-TMDs.[15] This mechanism is supported by earlier photothermal deflection spectroscopy of MoS_2 nanoflakes, where increased linear absorption at sub-bandgap energies was observed for large MoS_2 crystals after lithographic texturing that increased the total amount of edges in the sample.[16] s-TMD flakes prepared by liquid phase exfoliation (LPE) – a widely used technique for the low-cost, mass manufacture of nanomaterials – also have a high edge to surface area ratio, and are thus expected to exhibit sub-bandgap states, supporting absorption of photons with lower energies than the material bandgap. Recent studies have demonstrated that the sub-bandgap absorption in s-TMD nanoflakes can be saturated, and exploited this effect in the development of ultrafast lasers operating in the near-infrared, corresponding to photon energies in the range 0.6–1.12 eV.[7–12,15] While a growing body of experimental work continues to substantiate the process of sub-bandgap absorption in s-TMDs, and practical applications of this phenomenon are being leveraged in the field of photonics, theoretical analyses are limited and the origin of sub-bandgap optical absorption remains an open question. Here, we develop an analytical theory, testing the hypothesis of edge-mediated absorption in s-TMDs to explain the phenomenon of sub-bandgap saturable absorption.

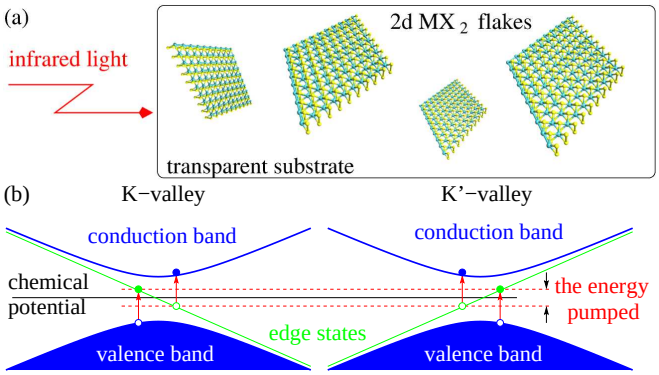

FIG. 1: (Color online.) (a) The s-TMD flakes are randomly distributed within a polymer substrate illuminated by infrared light with an excitation energy below the material bandgap. (b) The electronic band structure of a single flake includes conduction, valence and edge-states. The edge-states are one-dimensional, i.e. the depicted momentum axis is parallel to the flake's edge. There are two mirror copies of these bands in the first Brillouin zone (K and K' valley). For a given excitation energy two *independent* optical absorption channels are possible in each valley corresponding to the valence-to-edge and edge-to-conduction bands direct transitions. These transitions are shown by red arrows, and the electrons and holes created are depicted by the filled and empty circles, respectively. Each edge-state electron-hole pair accumulates a certain amount of energy which after thermalization appears as an elevated temperature for the edge-state electrons.

The electronic states at the edges of a nanoflake (edge-states) can be modeled starting from two opposing viewpoints. Firstly, by focusing on the atomic structure of a particular edge and computing the energy dispersion by means of a tight-binding model[17–20] (including its continuum limit[21,22]); secondly, using density functional theory (DFT).[23–25] Both approaches provide a quantitative description of the optical absorption of a particular flake with a given edge type; however, experimental measurements are typically preformed on an array of small flakes, randomly oriented in a polymer, with different edge types. To describe the ensemble of flakes we use an effective Hamiltonian, with a spatially dependent bandgap simulating the flake edge. A somewhat similar model is known in the literature as a neutrino billiard.[26] This model neglects the details of any particular edge but allows us to calculate the wave functions and the Fermi's golden-rule optical transitions from and to the edge-states analytically.

The peculiarities of the edge-state absorption are depicted in Fig. 1. In contrast to the two-band model for bulk semiconductors,[27] our approach involves *three* electron subsystems. A one-dimensional edge-state electron subsystem that always remains in the metallic regime with the Fermi energy determined by the bulk chemical potential. In contrast, the conduction and valence bands are in the semiconducting regime: the valence band is occupied almost completely whereas the conduction band is nearly empty. Subgap direct transitions occur between the valence band and edge states as well as the edge and conduction band states. The relative contribution of these two transitions is determined by Pauli blocking and depends on the relationship between the excitation frequency and the Fermi level. We show, that despite the complexity of the model, the saturable subgap absorption A^Φ for s-TMD flakes can be written in the conventional form[27]

$$A^\Phi = \frac{A}{1+\frac{\Phi}{\Phi^s}}, \tag{1}$$

where A is the relative linear absorption estimated by Eq. (17), Φ is the absorbed fluence, Φ^s is the saturation fluence given by Eq. (24). The absorption is defined as a ratio of the absorbed radiation fluence to the incident fluence. In the rest of the paper, we derive the analytical expressions for A and Φ^s, and analyze their behavior.

II. MODEL

From the point of view of the band theory the difference between semiconductor and vacuum can be described by means of the bandgap Δ: it is finite in the semiconducting region but infinite outside, where no conduction is possible. Let us consider a simple Hamiltonian derived for electrons on a honey-comb lattice using the tight-binding approach with the lattice constant a, the on-site energies $\epsilon_{A,B}$, and the nearest-neighbor hopping $t_\perp$. Near the K corner of the hexagonal first Brillouin zone the Hamiltonian can be written in the continuum limit as[28]

$$H_0^K = \begin{pmatrix} \epsilon_A & -t_\perp\frac{\sqrt{3}a}{2}(\hat{k}_x - i\hat{k}_y) \\ -t_\perp\frac{\sqrt{3}a}{2}(\hat{k}_x + i\hat{k}_y) & \epsilon_B \end{pmatrix},$$

where $\hat{k}_x = -i\partial_x$, $\hat{k}_y = -i\partial_y$ are momentum operators. (The Hamiltonian for K'-corner can be obtained by the substitution $\hat{k}_x \to -\hat{k}_x$.) This Hamiltonian can be rewritten in a more instructive form given by[29]

$$H_0^K = \text{const} + \begin{pmatrix} \frac{\Delta}{2} & \hbar v(\hat{k}_x - i\hat{k}_y) \\ \hbar v(\hat{k}_x + i\hat{k}_y) & -\frac{\Delta}{2} \end{pmatrix}, \tag{2}$$

where const $= (\epsilon_A + \epsilon_B)/2$, $\Delta = \epsilon_A - \epsilon_B$ represents the bandgap, and $-\sqrt{3}at_\perp/2 = \hbar v$, with $\hbar v = 1.1$ eV $\times$ 3.193Å for MoS_2.[29] The gap can be either positive or negative depending on the difference between the on-site energies $\epsilon_{A,B}$.

The edge-states along the x-axis can be simulated by means of a y-dependent gap $\Delta(y)$. We first solve the edge-state spectral problem for K-valley $H_0^K\psi_e = E_e\psi_e$ and obtain the eigen state wave function ψ_e in the form

$$\psi_e = C\exp\left(ik_x x - \int_0^y \frac{\Delta(y')dy'}{2\hbar v}\right)\begin{pmatrix}1\\-1\end{pmatrix}, \tag{3}$$

where C is a normalization constant, and $\Delta(y)$ should change its sign at $y = 0$.[30] (An edge along the y-axis can be modeled in a similar way by an x-dependent gap $\Delta(x)$.) Since we aim for an analytical derivation of the linear absorption and saturation fluence we simplify $\Delta(y)$ as

$$\Delta(y) = \begin{cases} \Delta > 0, & y \geq 0 \quad (\texttt{semiconductor}); \\ -\infty, & y < 0 \quad (\texttt{vacuum}). \end{cases} \tag{4}$$

Eq. (3) then reads

$$\psi_e = \sqrt{\frac{\Delta}{2L\hbar v}} \exp\left(ik_x x - \frac{y\Delta}{2\hbar v}\right) \begin{pmatrix} 1 \\ -1 \end{pmatrix}, \quad y \geq 0 \tag{5}$$

which is normalized as

$$\lim_{W\to\infty} \int_0^L dx \int_0^W dy (\psi_e^\dagger \psi_e) = 1,$$

and obeys the dispersion $E_e = -\hbar v k_x$. Due to Eq. (4), ψ_e exponentially vanishes in the bulk because $\Delta > 0$ at $y \geq 0$. Note that ψ_e equals to zero at $y < 0$ but is finite at $y = 0$, i.e. it demonstrates a step-like behavior. This is because $\Delta(y)$ is not a true electrostatic potential, as emphasized by Berry and Mondragon[26], but a "staggered" one.[18] Even if $\Delta(y)$ goes to infinity, it is not equivalent to the hard-wall potential, where the wave function must vanish at the border. For K'-valley, the solution of the spectral problem results in the same dispersion E_e but taken with an opposite sign (see Fig. 1b). In contrast to a topological quantum-Hall insulator,[30] the edge states (5) exist in two mirror copies in two valleys. To give an example, the edge-state electrons in MX_2 monolayers may experience intervalley backscattering, i.e. the edge-state electron transport is not topologically protected. It is worth emphasizing that our conclusions do not depend on whether the edge is along the x or y direction since the optical absorption is averaged over the flake orientation.

The bulk conduction band eigen wave functions for K-valley are given by

$$\psi_c = \frac{1}{\sqrt{LW}} \exp\left(ik_x x + ik_y y\right) \begin{pmatrix} \cos\frac{\theta}{2} \\ \sin\frac{\theta}{2} e^{i\phi} \end{pmatrix}, \tag{6}$$

with the dispersion $E_c = \sqrt{(\hbar v k)^2 + \Delta^2/4}$, whereas the valence band wave functions read

$$\psi_v = \frac{1}{\sqrt{LW}} \exp\left(ik_x x + ik_y y\right) \begin{pmatrix} \sin\frac{\theta}{2} \\ -\cos\frac{\theta}{2} e^{i\phi} \end{pmatrix}, \tag{7}$$

with the dispersion $E_v = -\sqrt{(\hbar v k)^2 + \Delta^2/4}$. Here,

$$\tan\theta = \frac{2\hbar v k}{\Delta}, \quad \tan\phi = \frac{k_y}{k_x}.$$

The bulk states are normalized to unity on the rectangle $0 \leq x \leq L$, $0 \leq y \leq W$.

The electron-photon interaction Hamiltonian for K-valley is derived from (2) and is given by[31,32]

$$H^{\rm int} = \frac{evE_0}{2\omega} \begin{pmatrix} 0 & e^{-i\theta_E} \\ e^{i\theta_E} & 0 \end{pmatrix},$$

where E_0, ω, and θ_E are the electromagnetic wave amplitude, frequency, and polarization angle correspondingly. The valence-to-edge states transitions are described by the following matrix element

$$\langle\psi_e|H^{\rm int}|\psi_v\rangle = -\sqrt{\frac{\Delta}{2\hbar W v}} \frac{evE_0}{2L\omega} \left(\cos\frac{\theta}{2} e^{i\phi - i\theta_E} + \right.$$
$$\left. + \sin\frac{\theta}{2} e^{i\theta_E}\right) \frac{e^{i(k_x - k_x')L} - 1}{i(k_x - k_x')} \frac{e^{\left(ik_y - \frac{\Delta}{2\hbar v}\right)W} - 1}{ik_y - \frac{\Delta}{2\hbar v}}. \tag{8}$$

Here, $(k_x, k_y) = \mathbf{k}$ and k_x' are momenta components in the bulk and at the edge, respectively. The valence-to-edge states transition rate can be calculated as

$$g_{ev}^{\rm ph}(\omega) = \sum_{k_x, k_y, k_x'} \frac{2\pi}{\hbar} |H_{ev}^{\rm int}|^2 \left(f_v^{(0)} - f_e^{(0)}\right) \tag{9}$$
$$\times\delta\left(-\hbar v k_x' + \sqrt{(\hbar v k)^2 + \Delta^2/4} - \hbar\omega\right),$$

where $f_v^{(0)}$, $f_e^{(0)}$ are the Fermi-Dirac distributions for electrons in the valence band and in the edge-states, respectively and $|H_{ev}^{\rm int}|^2$ reads

$$|H_{ev}^{\rm int}|^2 = \lim_{L,W\to\infty} |\langle\psi_e|H^{\rm int}|\psi_v\rangle|^2$$

$$= \frac{\Delta}{2\hbar v} \frac{2\pi}{LW} \delta(k_x - k_x') \left(\frac{evE_0}{2\omega}\right)^2 \frac{1 + \sin\theta\cos(\phi - 2\theta_E)}{\left(\frac{\Delta}{2\hbar v}\right)^2 + k_y^2}.$$

The edge-to-conduction band transition rate differs from Eq.(9) by the sign in front of the θ_E-dependent term and by the filling factors. The corresponding generation rate reads

$$g_{ce}^{\rm ph}(\omega) = \sum_{k_x, k_y, k_x'} \frac{2\pi}{\hbar} |H_{ce}^{\rm int}|^2 \tag{10}$$
$$\times\delta\left(\sqrt{(\hbar v k)^2 + \Delta^2/4} + \hbar v k_x' - \hbar\omega\right) \left(f_e^{(0)} - f_c^{(0)}\right),$$

where

$$|H_{ce}^{\rm int}|^2 = \lim_{L,W\to\infty} |\langle\psi_c|H^{\rm int}|\psi_e\rangle|^2$$

$$= \frac{\Delta}{2\hbar v} \frac{2\pi}{LW} \delta(k_x - k_x') \left(\frac{evE_0}{2\omega}\right)^2 \frac{1 - \sin\theta\cos(\phi - 2\theta_E)}{\left(\frac{\Delta}{2\hbar v}\right)^2 + k_y^2},$$

and $f_c^{(0)}$ stands for the conduction band Fermi-Dirac distribution.

The flakes are randomly oriented, thus, the relative optical absorption is determined by the ratio between

the θ_E-averaged absorbed power $\hbar\omega\langle g_{ev}^{\rm ph}+g_{ce}^{\rm ph}\rangle_{\theta_E}$ and the incident radiation power $(cE_0^2S)/(8\pi)$ with S being the illuminated area. To sum-up over k_x', k_x, and k_y we transform sums to integrals as

$$\sum_{k_x,k_y,k_x'}\to\int\frac{dk_x'L}{2\pi}\int\frac{dk_xL}{2\pi}\int\frac{dk_yW}{2\pi}.$$

The integral over k_x' is taken using the momentum conservation represented above as $\delta(k_x-k_x')$. The integral over k_x is then taken using the energy conservation utilizing the transformation

$$\delta\left(\sqrt{(\hbar vk)^2+\Delta^2/4}\pm\hbar vk_x-\hbar\omega\right)=$$

$$=\frac{\hbar^2\omega^2+\Delta^2/4+\hbar^2v^2k_y^2}{2\hbar^3\omega^2v}\times$$

$$\times\delta\left(k_x\mp\frac{\hbar^2\omega^2-\Delta^2/4-\hbar^2v^2k_y^2}{2\hbar^2\omega v}\right).$$

We then substitute $\hbar vk_y=\varepsilon$, $E_\omega=\hbar\omega$ and obtain the relative absorption of a single edge A_1 in the form $A_1=A_1^++A_1^-$, where $A_1^\pm$ correspond to the $v\to e$ and $e\to c$ transitions, respectively and are given by

$$A_1^\pm=\frac{e^2}{\hbar c}\frac{\hbar vL}{S}\frac{\Delta}{4E_\omega}\int\limits_{-\infty}^{\infty}d\varepsilon\left(\frac{1}{E_\omega^2}+\frac{1}{\varepsilon^2+\Delta^2/4}\right)F^\pm(\varepsilon). \tag{11}$$

Here, $F^\pm(\varepsilon)$ describe the corresponding occupations and are given by

$$F^+(\varepsilon)=\frac{1}{1+\exp\left(-\frac{\varepsilon^2+\Delta^2/4+E_\omega^2}{2E_\omega T_0}-\frac{\mu_p}{T_0}\right)}$$
$$-\frac{1}{1+\exp\left(-\frac{\varepsilon^2+\Delta^2/4-E_\omega^2}{2E_\omega T}-\frac{\mu}{T}\right)}, \tag{12}$$
$$F^-(\varepsilon)=\frac{1}{1+\exp\left(\frac{\varepsilon^2+\Delta^2/4-E_\omega^2}{2E_\omega T}-\frac{\mu}{T}\right)}$$
$$-\frac{1}{1+\exp\left(\frac{\varepsilon^2+\Delta^2/4+E_\omega^2}{2E_\omega T_0}-\frac{\mu_n}{T_0}\right)}. \tag{13}$$

Here, we set different (fluence dependent) quasi Fermi levels[33] μ_n and μ_p for the conduction and valence bands correspondingly. The quasi Fermi levels μ_n and μ_p are both equal to the equilibrium chemical potential μ as long as no interband transitions occur and no photocarriers are excited. These notations will be utilized in section IV devoted to the saturable absorption. Moreover, two temperatures have been introduced: T_0 is the lattice temperature for bulk electrons, and T is the temperature for edge-state electrons which may differ from T_0 in some cases described in section V.

We emphasize that Eq. (11) describes the optical absorption of a *single* edge of a *single* flake for a *given* spin and valley channel. The total absorption of a s-TMD dispersion or a s-TMD-polymer composite should take into account different spin and valley channels as well as the concentration of flakes. It can be shown that the K'-valley edge states result in the same contribution to the absorption as (11). The spin-split absorption channels give two different contributions determined by the spin-dependent bandgap value $\Delta=\Delta_s$, but we neglect the spin splitting for the sake of simplicity. Moreover, we assume that the flakes are squares of the size d, and all flakes are placed perpendicular to the light beam. To sum up these contributions, we define an *effective* length as

$$L^{\rm eff}=\ell S\quad\text{with}\quad\ell=4dg_{sv}n_{2D}, \tag{14}$$

where $4d$ is the average perimeter of a flake, $g_{sv}=4$ is the spin/valley degeneracy, and n_{2D} is the number of monolayer flakes per unit area of a composite film. The quantity ℓ then plays a role of the total effective length of monolayer flakes' edges per unit area of a composite film. Assuming the size of the flake to be of the order of 100nm, the monolayer flake concentration $n_{2D}\sim10^{11}\,{\rm cm}^{-2}$ we estimate the effective length to be of the order of 1km for a 1mm^2 spot-size. In order to convert the absorption of a single edge (11) to the total absorption of a composite we make the substitution $L\to L^{\rm eff}$, i.e. $A=A_1(L\to L^{\rm eff})$. Eq. (11) is the main results of this work. It can be used to calculate the linear and nonlinear absorption. We now elaborate on these two cases.

III. LINEAR ABSORPTION

In the low-fluence limit we set the valence band occupation to 1 (completely filled) and the conduction band occupation to 0 (completely empty). Eq.(11) can be then written as

$$A_1^\pm(T)=\frac{e^2}{\hbar c}\frac{\hbar vL}{S}\frac{\Delta}{4E_\omega}\int\limits_{-\infty}^{\infty}d\varepsilon\left(\frac{1}{E_\omega^2}+\frac{1}{\varepsilon^2+\Delta^2/4}\right)$$
$$\times\frac{1}{1+\exp\left(\frac{\varepsilon^2+\Delta^2/4-E_\omega^2}{2E_\omega T}\pm\frac{\mu}{T}\right)}. \tag{15}$$

In the intrinsic semiconductor limit ($\mu=0$) both terms $A_1^\pm$ are the same. If all the energies involved (i.e. E_ω, Δ, and μ) are much higher than the temperature, then we can take the limit of $T=0$, and the absorption reads

$$A_1^\pm(0)=\frac{e^2}{\hbar c}\frac{\hbar vL}{S}\frac{\Delta}{2E_\omega}\left[\frac{\sqrt{E_\omega^2\pm2\mu E_\omega-\Delta^2/4}}{E_\omega^2}\right.$$
$$\left.+\frac{2}{\Delta}\arctan\left(\frac{\sqrt{E_\omega^2\pm2\mu E_\omega-\Delta^2/4}}{\Delta/2}\right)\right]. \tag{16}$$

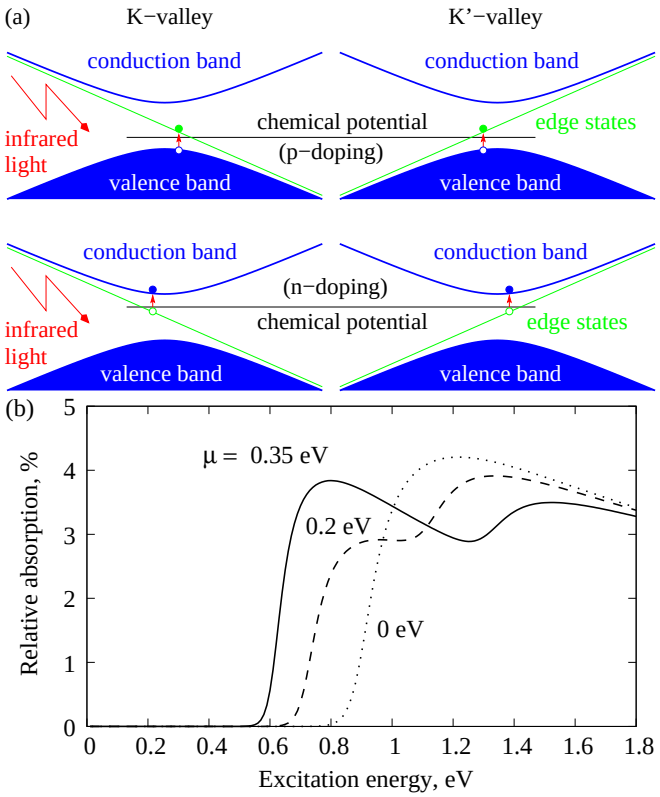

FIG. 2: (a) (Color online.) The possible direct optical transitions at a given radiation wavelength in doped samples. Since the bands are symmetric there is no difference, whether the flakes are n- or p-doped. (b) Relative linear optical absorption of $5.64 \cdot 10^{11}$ cm^{-2} monolayer MoS_2 flakes at room temperature. The excitonic and direct valence-to-conduction interband transitions relevant at the excitation energies near Δ are not taken into account. The flakes are n-doped with the chemical potential ranging from 0 to 0.35 eV. The average flake size is 90 nm, the bandgap is 1.8 eV, the band parameter is $\hbar v = 1.1\text{eV} \times 3.193\text{Å}$.[29] The spin-orbit splitting is neglected.

Eq. (16) is applicable only when the square roots are real, the corresponding terms should be set to zero otherwise. Physically, vanishing absorption corresponds to the Pauli blocking depicted in Fig. 2a.

The total linear absorption of a composite can be obtained by making the substitution $L \to L^{\text{eff}}$ and is shown in Fig. 2b as a function of the excitation energy. To be specific, we consider the n-doped samples ($\mu > 0$). The opposite case of $\mu < 0$ results in the same behavior since the bands are assumed to be symmetric with respect to $E = 0$ (the middle of the bandgap). At too low excitation energies (when $E_\omega^2 + 2\mu E_\omega - \Delta^2/4 < 0$) the absorption vanishes. Increasing the excitation energy we first activate the transitions from the edge states to the conduction band. This results in the relative absorption of about 4% for the s-TMD–composite we consider. The absorption decreases slightly with the excitation wavelength until the transitions from the valence band to the edge states becomes activated at $E_\omega^2 - 2\mu E_\omega - \Delta^2/4 > 0$. The dependence $A(E_\omega)$ is therefore non-monotonic due to the different absorption channels opened at different E_ω. Note that the bands in real MX_2 samples are spin-split; therefore, we expect each of two maxima in $A(E_\omega)$ to split into two that results in a somewhat more complicated pattern. At low doping ($\mu \to 0$) the two maxima merge into a single absorption maximum at E_ω near $\Delta/2$. Considering Eq. (16) in this limit we can roughly estimate the total linear absorption of a composite film as

$$A \sim \frac{4e^2}{\hbar c}\frac{\hbar v}{\Delta}\ell, \tag{17}$$

where ℓ is defined in (14). The physical meaning is clear: the absorption is larger for smaller Δ because the real-space width of the edge state (5) is larger for smaller gaps. The absorption is proportional to the total length of edges ℓ (per unit square) involved in the absorption. Substituting parameters relevant for MoS_2,[29] and using $d \approx 100$nm and $n_{2D} \approx 5{\cdot}10^{11}$ cm^{-2}, we obtain the subgap absorption of the order of 1%.

IV. SATURABLE ABSORPTION

If the incident fluence Φ is close to the saturation fluence, then the quasi Fermi energies μ_n and μ_p should be taken into account. They can be calculated using the particle conservation. On the one hand, the photocarrier concentration in the conduction band due to the single-edge absorption is $n^{\text{ph}} = \Phi A_1^-/E_\omega$, where A_1^- is the edge-to-conduction band absorption, see Eq. (11). On the other hand, the same concentration can be calculated for the thermalized electrons as

$$n^{\text{ph}} = \int \frac{d^2k}{4\pi^2} \frac{1}{1+\exp\left(\frac{\sqrt{(\hbar v k)^2+\Delta^2/4}-\mu_n}{T_0}\right)}$$

$$\approx \frac{T_0\Delta}{4\pi\hbar^2 v^2} e^{\frac{\mu_n-\Delta/2}{T_0}}, \tag{18}$$

This approximation is valid as long as $(\Delta/2-\mu_n)/T_0 \gg 1$. Thus, μ_n can be determined from

$$e^{\frac{\mu_n}{T_0}} = \frac{4\pi\hbar^2 v^2}{T_0\Delta}\frac{\Phi A_1^-}{E_\omega} e^{\frac{\Delta}{2T_0}}. \tag{19}$$

The quasi Fermi energy for the valence band μ_p is calculated in the same way using the photoexcited hole concentration $p^{\text{ph}} = \Phi A_1^+/E_\omega$ and its thermalized version, which reads

$$p^{\text{ph}} = \int \frac{d^2k}{4\pi^2}\left(1 - \frac{1}{1+\exp\left(\frac{-\sqrt{(\hbar v k)^2+\Delta^2/4}-\mu_p}{T_0}\right)}\right)$$

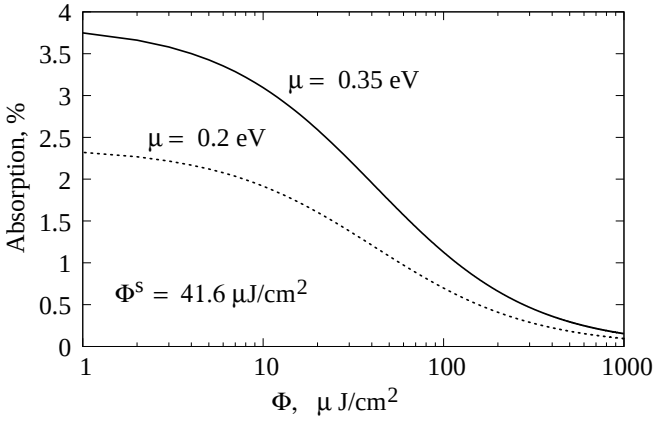

FIG. 3: Saturable optical absorption of a MoS_2 composite at $E_\omega = 0.8$ eV. The parameters are the same as in Fig. 2. The saturation fluence is estimated from Eq. (IV) with $L \to L^{\rm eff}$, but Eq. (24) gives nearly the same result for Φ^s of about $40\,\mu$J/cm^2. It corresponds to the intensity of a few MW/cm^2 at the electron-hole recombination time of the order of 10 ps, see Ref.[34]

$$\approx \frac{T_0\Delta}{4\pi\hbar^2 v^2} e^{-\frac{\mu_p+\Delta/2}{T_0}}. \qquad (20)$$

Note, that $\mu_p < 0$. Hence, μ_p can be found from

$$e^{-\frac{\mu_p}{T_0}} = \frac{4\pi\hbar^2 v^2}{T_0\Delta}\frac{\Phi A_1^+}{E_\omega} e^{\frac{\Delta}{2T_0}}. \qquad (21)$$

Now, we employ Eqs. (12,13) assuming that

$$\frac{1}{1+\exp\left(-\frac{\varepsilon^2+\Delta^2/4+E_\omega^2}{2E_\omega T_0}-\frac{\mu_p}{T_0}\right)}$$

$$\approx 1-\exp\left(-\frac{\varepsilon^2+\Delta^2/4+E_\omega^2}{2E_\omega T_0}-\frac{\mu_p}{T_0}\right),$$

$$\frac{1}{1+\exp\left(\frac{\varepsilon^2+\Delta^2/4+E_\omega^2}{2E_\omega T_0}-\frac{\mu_n}{T_0}\right)}$$

$$\approx \exp\left(-\frac{\varepsilon^2+\Delta^2/4+E_\omega^2}{2E_\omega T_0}+\frac{\mu_n}{T_0}\right),$$

and exclude $\mu_{n,p}$ using Eqs. (19,21). These approximations are standard for semiconductors: we substitute the electron and hole Fermi-Dirac occupations by the corresponding Boltzmann distributions. Note, that the edge states are in the metallic regime and, therefore, the Fermi-Dirac distribution must be retained for this subsystem. To take the integral over ε we calculate the following expressions:

$$\int_{-\infty}^{\infty}\frac{d\varepsilon}{E_\omega^2}\exp\left(-\frac{\varepsilon^2+\Delta^2/4+E_\omega^2}{2E_\omega T_0}+\frac{\Delta}{2T_0}\right)$$

$$=\frac{1}{E_\omega}\sqrt{\frac{2\pi T_0}{E_\omega}}\exp\left[-\frac{(E_\omega-\Delta/2)^2}{2E_\omega T_0}\right],$$

$$\int_{-\infty}^{\infty}\frac{d\varepsilon}{\varepsilon^2+\Delta^2/4}\exp\left(-\frac{\varepsilon^2+\Delta^2/4+E_\omega^2}{2E_\omega T_0}+\frac{\Delta}{2T_0}\right)$$

$$=\frac{2\pi}{\Delta}\exp\left(\frac{\Delta-E_\omega}{2T_0}\right)\mathrm{Erfc}\left(\frac{\Delta}{\sqrt{8E_\omega T_0}}\right),$$

where Erfc is the complementary error function. After some algebra we obtain the saturable absorption in the form

$$A_1^\Phi = \frac{A_1(T)}{1+\frac{\Phi}{\Phi_1^s}}, \qquad (22)$$

where $A_1(T) = A_1^+ + A_1^-$ is the linear absorption with $A_1^\pm$ given by Eq. (III). The saturation fluence Φ_1^s can be found from

$$\frac{1}{\Phi_1^s} = \frac{\pi e^2}{\hbar c}\frac{\hbar^3 v^3 L}{E_\omega^3 T_0 S}\exp\left[-\frac{(E_\omega-\Delta/2)^2}{2E_\omega T_0}\right]$$

$$\times\left[\sqrt{\frac{2\pi T_0}{E_\omega}}+\frac{2\pi E_\omega}{\Delta}e^{\frac{\Delta^2}{8E_\omega T_0}}\mathrm{Erfc}\left(\frac{\Delta}{\sqrt{8E_\omega T_0}}\right)\right]. \qquad (23)$$

If we neglect the heating of the edge state electrons, then we can set $T = T_0$ in Eq. (III), and $A_1^\pm(T)$ can be approximated by $A_1^\pm(0)$ given by Eq. (16). The nonlinear absorption A_1^Φ will be then determined solely by the $(1+\Phi/\Phi_1^s)^{-1}$ multiplier, as if it is the standard two-band model.[27] In order to find the total composite absorption we make the substitution $L \to L^{\rm eff}$ in (22) and obtain our main result (1) with $\Phi^s = \Phi_1^s(L \to L^{\rm eff})$ and $A = A_1(L \to L^{\rm eff})$.

We show the composite nonlinear absorption A^Φ in Fig. 3 at the telecommunication wavelength of 1550 nm ($E_\omega = 0.8$ eV). The incident fluence can be translated to the intensity as $I = \Phi/\tau$ with τ being the electron-hole recombination time of about 10 ps, see Ref.[34] The saturation fluence evaluated from (IV) in the excitation energy range 0.8–1.0 eV is of the order of $10\,\mu$J/cm^2 that corresponds to the intensity of the order of 10^6 J/(s $\cdot$ cm^2), relevant for the typical measurements.[11] Eq. (IV) also suggests, that the saturation intensity increases dramatically at the excitation energies far from $\Delta/2$. Physically, the half of the bandgap $\Delta/2$ plays the same role in our approach as the true bandgap Δ in the conventional two-band model.[27] The saturation is most efficient when the photocarriers are excited from and to the band edges. Our model is entering into this regime when the excitation energy is near $\Delta/2$, as one can see from Fig. 1. At the excitation energies much higher than $\Delta/2$ the photocarriers are excited far from the conduction and valence

band edges and cannot be described by a thermalized distributions (19) and (21). It is instructive to consider the limit $E_\omega = \Delta/2$ and subsequently assume that $\Delta \gg T_0$. The second term in Eq. (IV) can be then approximated as $\pi e^{\frac{\Delta}{4T_0}} \mathrm{Erfc}\left(\sqrt{\frac{\Delta}{4T_0}}\right) \approx \sqrt{\frac{4\pi T_0}{\Delta}}$, and the final formula for the composite saturation fluence reads

$$\frac{1}{\Phi^s} \sim \frac{4\pi^{\frac{3}{2}} e^2}{\hbar c} \frac{\hbar^3 v^3 \ell}{E_\omega^3 \sqrt{\Delta T_0}}, \tag{24}$$

where $E_\omega \sim \Delta/2$. The absorption is therefore easier to saturate at smaller gap Δ and longer effective edge length defined in (14).

V. HOT ELECTRONS ON EDGES

The situation becomes more complicated at the excitation energies higher than half the bandgap ($E_\omega > \Delta/2$) in the intrinsic semiconductor regime ($\mu = 0$). The energy necessary to promote one edge-state electron to the conduction band (or an edge-state hole to the valence band) is $\Delta/2$. The question we address in this section is what happens with the excess energy $E_\omega - \Delta/2$ after each excitation event.

As already shown in Fig.1b, two independent excitation channels corresponding to the valence-to-edge and edge-to-conduction band transitions are opened. The valence-to-edge state transitions promote electrons to just above the Fermi level at the same rate as the edge-to-conduction state transitions create holes just below the Fermi energy, see Fig. 1b. Effectively, these transitions lift an electron from an edge state below μ to another edge state above μ. If the radiation intensity is high enough (the excitation is faster than the interband recombination), then this results in the generation of electron-hole pairs *within the edge-state subsystem*. Since electron-electron collisions are very efficient in a one-dimensional case the edge-state electron occupation quickly thermalizes to a Fermi-Dirac distribution with an elevated temperature. Thus, the excess energy is accumulated by the edge-state electrons. Let us quantify this mechanism.

To calculate this temperature we have to solve the energy balance equation with respect to T:

$$\delta E + E_n + E_p = A_1 S \Phi. \tag{25}$$

The right-hand side of (25) is the absorbed energy which is balanced with the energies δE, E_n, E_p accumulated by the thermalized edge, conduction and valence band electrons. The last two can be estimated as $E_n \approx A_1^- S\Phi\Delta/2E_\omega$ and $E_p \approx A_1^+ S\Phi\Delta/2E_\omega$, where the same approximation as in eqs. (18), (20) has been utilized. The energy pumped into the edge-state electron gas can be calculated assuming that the occupation is already thermalized and given by the Fermi-Dirac distribution function. The edge-state electron-hole excitation energy

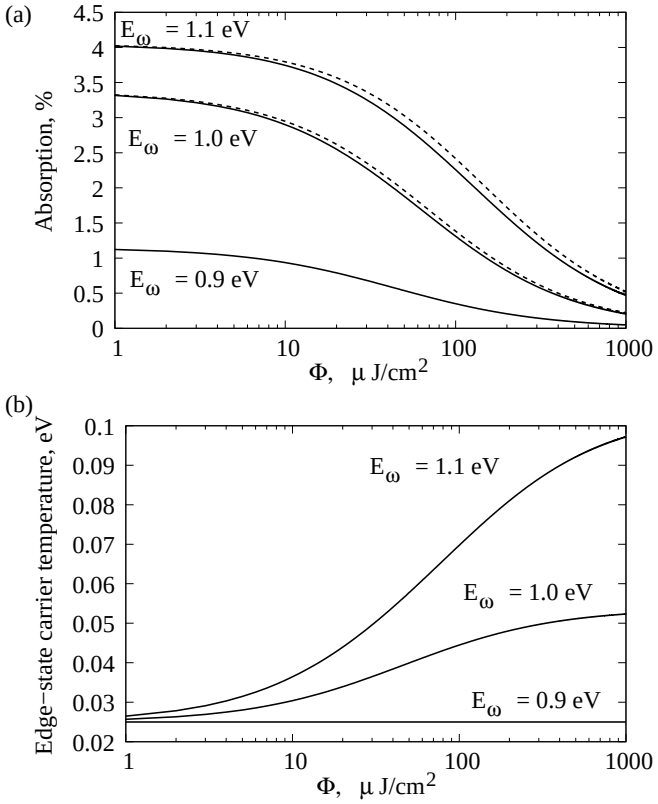

FIG. 4: (a) Saturable absorption in the intrinsic limit ($\mu = 0$) at different excitation energies $E_\omega \geq \Delta/2$. The dashed curves correspond to the simplified model where the edge-state electron temperature remains constant. The solid curves take into account the energy pumping due to the processes shown in Fig. 1b. At the excitation energies higher than $\Delta/2$, the deviation between the solid and dashed curves is clearly visible. (b) Edge-state electron temperature *vs.* fluence computed from (V).

is the difference between the electron and hole energies within the edge-state band, as shown in Fig. 1b by dashed lines. It can be written as

$$\begin{aligned} E(T) &= \int\limits_{-\infty}^{-\frac{\mu}{\hbar v}} \frac{dk_x L}{2\pi} \frac{-\hbar v k_x}{1+\exp\left(\frac{-\hbar v k_x - \mu}{T}\right)} \\ &- \int\limits_{-\frac{\mu}{\hbar v}}^{\infty} \frac{dk_x L}{2\pi} \frac{-\hbar v k_x}{1+\exp\left(\frac{\hbar v k_x + \mu}{T}\right)} \\ &= \frac{\pi T^2 L}{12\hbar v}. \end{aligned} \tag{26}$$

Since the one-dimensional edge-state density of states is a constant in our model $E(T)$ does not depend on μ, and δE reads

$$\delta E = \frac{\pi L}{12\hbar v}(T^2 - T_0^2). \tag{27}$$

Eq. (25) is then written as

$$\frac{\pi(T^2-T_0^2)}{12\hbar v}\frac{L}{S}=\left(1-\frac{\Delta}{2E_\omega}\right)\Phi A_1. \tag{28}$$

Substituting $L\to L^{\rm eff}$, $A_1\to A^\Phi$ we obtain the following equation for the edge-state electron temperature in a composite:

$$T^2-T_0^2=\frac{3\hbar e^2v^2\Phi\Delta}{\pi cE_\omega}\frac{1-\Delta/(2E_\omega)}{1+\Phi/\Phi^s}$$

$$\times\sum_{\pm}\int_{-\infty}^{\infty}d\varepsilon\frac{(E_\omega)^{-2}+\left(\varepsilon^2+\Delta^2/4\right)^{-1}}{1+\exp\left(\frac{\varepsilon^2+\Delta^2/4-E_\omega^2}{2E_\omega T}\pm\frac{\mu}{T}\right)}. \tag{29}$$

This equation can be solved with respect to T numerically using the method of iterations (the method of consecutive approximations). The result is demonstrated in Fig. 4, where absorption and edge-state carrier temperature are shown for different excitation energies. If $E_\omega=\Delta/2$, then the solid and dashed curves coincide, and heating of the edge-state electrons (solid curve) can be neglected. If $E_\omega>\Delta/2$, then the excess energy $E_\omega-\Delta/2$ is pumped into the edge-state electron subsystem and its temperature can reach 0.1 eV ($\sim$ 1200 K). The high temperature makes the edge-states evenly populated in k_x-space that results in less electrons excited from the edge-states to the conduction band and less empty space available for the electrons coming from the valence band. Hence, the elevated temperature slightly reduces absorption, as shown in Fig. 4.

VI. CONCLUSION AND OUTLOOK

In conclusion, we have developed a simple model to qualitatively describe edge-state mediated absorption in s-TMD flakes and s-TMD-polymer composites. We show that the appropriate description must involve a three-level system, in contrast to the conventional two-band model routinely used for semiconductors.[27] At excitation energies near $\Delta/2$, the linear absorption of a s-TMD composite can be estimated using Eq. (17), while the saturation fluence is given by Eq. (24). The band structure parameters in Eqs. (17,24) can be calculated[29,35] or measured.[36] Our estimates of linear and saturable absorption agree, to within one order of magnitude, with existing saturable absorption measurements performed on WS_2[9] and $MoSe_2$[11,12] composites. We stress that this work does not aim at a quantitative analysis of specific samples. For this, the following should be considered:

- Due to the spin-orbit splitting in the valence band, the bandgap is different for each spin channel. Strictly speaking, we have *four* terms in the absorption $A^+_\uparrow$, $A^-_\uparrow$, $A^+_\downarrow$, $A^-_\downarrow$ instead of two $A^\pm$ considered here. The non-monotonic dependence of the linear absorption on the excitation energy shown in Fig. 2 becomes more complicated once we take into account of the spin-splitting.

- The light beam is assumed to be normal to the flakes. The plane of incidence is therefore not well defined; consequently, our model is insensitive to s- and p-polarization. This is not the case in real MX_2 composites where flakes are randomly oriented within the host polymer matrix. The quantitative model should therefore include averaging not only over the azimuthal polarization angle θ_E performed here, but also over the polar angle, as described in.[37]

- The majority of the experimental examples of s-TMDs for ultrafast photonics exploit ultrasonic or shear assisted LPE of their bulk crystals.[38] Such dispersions and composites mostly contain few-layer crystals.[7,11,39] In our model, we assume that the interlayer coupling is weak for the flakes produced by LPE, and any thin N-layer flake can be viewed as a stack of N monolayers, without such coupling. This approach works well for graphene,[40] but a quantitative model for s-TMDs should address this more carefully.

- Our formula for saturation fluence (IV) is not reliable for excitation energies far from $\Delta/2$. This is because at such energies the photocarriers are excited far from the band edges and cannot be described by a thermalized distribution used here. In order to improve the reliability of the model a non-thermalized distribution for conduction and valence band photocarriers should be employed.

- To calculate the hot electron temperature, we assume that there is no energy dissipation at the time scale of the incident pump pulse duration or the electron-hole recombination process, whichever is shorter. A quantitative model should include an additional term in the energy balance equation (25) to take into account energy relaxation.

- The model neglects defects in crystals completely. These defects could result in an additional non-saturable term in Eq. (1) for the nonlinear absorption A^Φ.

In addition to MX_2 flakes, our model could be applied to other hexagonal, nanostructured composites, e.g. boron nitride (h-BN) monolayers, where the bandgap size $\Delta=3.92$ eV and the bandgap parameter $\hbar v=2.33\text{eV}\times 2.174\text{Å}$.[41] This results in lower edge-state absorption, but the optimum excitation energy $E_\omega\approx\Delta/2$ lies in the visible region, near the wavelength of 630nm, suggesting h-BN may also be a suitable platform for the design of nonlinear composite-based devices in the visible spectral range.

VII. ACKNOWLEDGMENTS

The authors thank R. I. Woodward, R. C. T. Howe, G. Hu, and W. Belzig for fruitful discussions. EJRK and TH acknowledge funding support from the Royal Academy of Engineering. M.T. thanks SFB 767 for support.

[1] A. K. Geim, Rev. Mod. Phys. **83**, 851 (2011).
[2] M. Xu, T. Liang, M. Shi, and H. Chen, Chemical Reviews **113**, 3766 (2013).
[3] Q. H. Wang, K. Kalantar-Zadeh, A. Kis, J. N. Coleman, and M. S. Strano, Nature nanotechnology **7**, 699 (2012).
[4] K. F. Mak, C. Lee, J. Hone, J. Shan, and T. F. Heinz, Phys. Rev. Lett. **105**, 136805 (2010).
[5] T. Korn, S. Heydrich, M. Hirmer, J. Schmutzler, and C. Schüller, Applied Physics Letters **99**, 102109 (2011).
[6] A. Splendiani, L. Sun, Y. Zhang, T. Li, J. Kim, C.-Y. Chim, G. Galli, and F. Wang, Nano Letters **10**, 1271 (2010).
[7] M. Zhang, R. Howe, R. I. Woodward, E. J. Kelleher, F. Torrisi, G. Hu, S. Popov, J. Taylor, and T. Hasan, Nano Research **8**, 1522 (2015).
[8] R. Woodward, E. Kelleher, R. Howe, G. Hu, F. Torrisi, T. Hasan, S. Popov, and J. Taylor, Optics Express **22**, 31113 (2014).
[9] M. Zhang, G. Hu, G. Hu, R. Howe, L. Chen, Z. Zheng, and T. Hasan, Scientific Reports **5**, 17482 (2015).
[10] D. Mao, Y. Wang, C. Ma, L. Han, B. Jiang, X. Gan, S. Hua, W. Zhang, T. Mei, and J. Zhao, Scientific reports **5** (2015).
[11] R. I. Woodward, R. C. T. Howe, T. H. Runcorn, G. Hu, F. Torrisi, E. J. R. Kelleher, and T. Hasan, Opt. Express **23**, 20051 (2015).
[12] Z. Luo, Y. Li, M. Zhong, Y. Huang, X. Wan, J. Peng, and J. Weng, Photonics Research **3**, A79 (2015).
[13] Y. Zhang, T.-R. Chang, B. Zhou, Y.-T. Cui, H. Yan, Z. Liu, F. Schmitt, J. Lee, R. Moore, Y. Chen, et al., Nature nanotechnology **9**, 111 (2014).
[14] S. Wang, H. Yu, H. Zhang, A. Wang, M. Zhao, Y. Chen, L. Mei, and J. Wang, Advanced materials **26**, 3538 (2014).
[15] R. I. Woodward, R. C. T. Howe, G. Hu, F. Torrisi, M. Zhang, T. Hasan, and E. J. R. Kelleher, Photon. Res. **3**, A30 (2015).
[16] C. Roxlo, R. Chianelli, H. Deckman, A. Ruppert, and P. Wong, Journal of Vacuum Science & Technology A **5**, 555 (1987).
[17] L. Brey and H. A. Fertig, Phys. Rev. B **73**, 235411 (2006).
[18] A. R. Akhmerov and C. W. J. Beenakker, Phys. Rev. B **77**, 085423 (2008).
[19] J. Lado, N. Garcia-Martinez, and J. Fernandez-Rossier, Synthetic Metals **210**, 56 (2015).
[20] S. Pavlović and F. M. Peeters, Phys. Rev. B **91**, 155410 (2015).
[21] C. G. Péterfalvi, A. Kormányos, and G. Burkard, Phys. Rev. B **92**, 245443 (2015).
[22] C. Segarra, J. Planelles, and S. E. Ulloa, arXiv:1511.00866 [cond-mat.mes-hall] (2015).
[23] M. V. Bollinger, K. W. Jacobsen, and J. K. Norskov, Phys. Rev. B **67**, 085410 (2003).
[24] A. Vojvodic, B. Hinnemann, and J. K. Nørskov, Phys. Rev. B **80**, 125416 (2009).
[25] E. Erdogan, I. Popov, A. Enyashin, and G. Seifert, The European Physical Journal B **85**, 33 (2012).
[26] M. V. Berry and R. J. Mondragon, Proceedings of the Royal Society of London A: Mathematical, Physical and Engineering Sciences **412**, 53 (1987).
[27] E. Garmire, Selected Topics in Quantum Electronics, IEEE Journal of **6**, 1094 (2000).
[28] E. McCann, *Graphene Nanoelectronics: Metrology, Synthesis, Properties and Applications, chapter 8* (Springer-Verlag Berlin Heidelberg, 2012).
[29] D. Xiao, G.-B. Liu, W. Feng, X. Xu, and W. Yao, Phys. Rev. Lett. **108**, 196802 (2012).
[30] M. Z. Hasan and C. L. Kane, Rev. Mod. Phys. **82**, 3045 (2010).
[31] M. Trushin, A. Grupp, G. Soavi, A. Budweg, D. De Fazio, U. Sassi, A. Lombardo, A. C. Ferrari, W. Belzig, A. Leitenstorfer, et al., Phys. Rev. B **92**, 165429 (2015).
[32] M. Trushin and J. Schliemann, EPL (Europhysics Letters) **96**, 37006 (2011).
[33] J. Nelson, *The Physics of Solar Cells* (Imperial College Press, 2004).
[34] H. Wang, C. Zhang, and F. Rana, Nano Letters **15**, 8204 (2015).
[35] A. Kormányos, G. Burkard, M. Gmitra, J. Fabian, V. Zólyomi, N. D. Drummond, and V. Fal'ko, 2D Materials **2**, 022001 (2015).
[36] B. S. Kim, J.-W. Rhim, B. Kim, C. Kim, and S. R. Park, arXiv:1601.01418 [cond-mat.mes-hall] (2016).
[37] K. R. Paton and J. N. Coleman, arXiv:1511.04410 [cond-mat.mes-hall] (2015).
[38] R. C. Howe, G. Hu, Z. Yang, and T. Hasan, in *Proc. SPIE 9553, Low-Dimensional Materials and Devices* (2015), p. 95530R.
[39] R. C. Howe, R. I. Woodward, G. Hu, Z. Yang, E. J. Kelleher, and T. Hasan, physica status solidi (b) (2016).
[40] Z. Sun, T. Hasan, F. Torrisi, D. Popa, G. Privitera, F. Wang, F. Bonaccorso, D. M. Basko, and A. C. Ferrari, ACS Nano **4**, 803 (2010).
[41] R. M. Ribeiro and N. M. R. Peres, Phys. Rev. B **83**, 235312 (2011).